CHEMISTRY OF MATERIALS

Article

pubs.acs.org/cm

Integrative Approach toward Uncovering the Origin of Photoluminescence in Dual Heteroatom-Doped Carbon Nanodots

Yuri Choi,[†] Byungkyun Kang,[‡] Jooyong Lee,[§] Sunghu Kim,[‡] Gyeong Tae Kim,[§] Hyunju Kang,[§] Bo Ram Lee,[∥] Hajin Kim,[§,⊥] Sang-Hee Shim,[#] Geunsik Lee,[‡] Oh-Hoon Kwon,[‡,⊥] and Byeong-Su Kim*[,†,‡]

[†]Department of Energy Engineering, [‡]Department of Chemistry, and [§]Department of Biomedical Engineering, Ulsan National Institute of Science and Technology (UNIST), Ulsan 44919, Korea

[∥]Cavendish Laboratory, Department of Physics, University of Cambridge, J. J. Thomson Avenue, Cambridge CB30HE, United Kingdom

[⊥]Center for Soft and Living Matter, Institute for Basic Science (IBS), Ulsan 44919, Korea

[#]Department of Chemistry, Korea University, Seoul 02841, Korea

Supporting Information

ABSTRACT: The pursuit of exceptionally high photoluminescence (PL) and stability is critical in the development of novel fluorophores for use in challenging bioimaging and optoelectronic devices. Carbon nanodots (CDs) doped with heteroatoms provide a particularly attractive means of effectively tailoring their intrinsic properties and exploiting new phenomena. Here, we report a one-step, scalable synthesis of boron-and-nitrogen co-doped CD (BN-CD) with outstanding optical properties unlike those of nitrogen-doped CD (N-CD) in solid state as well as solution. The detailed mechanistic framework was explored using a series of spectroscopic analyses and ultrafast spectroscopy coupled with density functional theory calculations, which all conclusively confirmed that the presence of more graphitic structures in the core and well-distributed surface states are responsible for the enhanced PL in BN-CD. Furthermore, single-molecule spectroscopy analysis demonstrated that a single BN-CD shows higher PL intensity and enhanced photobleaching time. We anticipate that this study will aid in uncovering the full potential of CDs in various fields.

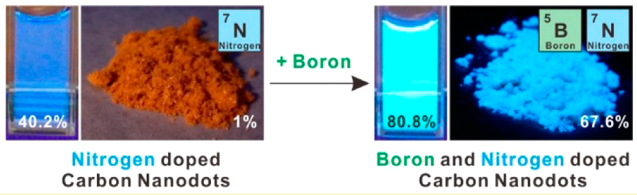

INTRODUCTION

Carbon-based nanomaterials, including graphene, carbon nanotube, fullerene, and carbon nanodots, have attracted significant attention because of their unique physical and chemical properties and their potential applications in a wide array of fields.[1] In particular, carbon nanodots (CDs) have emerged as a new class of optical materials by virtue of their interesting physical, optical, and chemical properties.[2,3] Their facile synthetic nature together with high photoluminescence (PL), photostability, and biocompatibility have triggered the recent development of CDs as a benign alternative to conventional semiconducting quantum dots.[4,5] Significant research efforts have focused on producing CDs with controlled dimensions and surface properties, using a variety of synthetic methods.[6−8] Despite this recent progress, the wide range of synthetic protocols often complicates the interpretation of the photophysical aspects of CDs because the synthetic precursor, synthetic method, and post-treatment can strongly influence these properties. In particular, the mechanism of PL from CDs has not been elucidated conclusively yet; for example, the quantum confinement effect, surface defects, functional groups, and degree of passivation on the surface have been proposed as the origin of PL in CDs.[9−12] This limitation in understanding of the origin of the PL poses a challenge for future development in the field.

Tailoring carbon nanomaterials with heteroatoms can effectively tune their electronic and chemical properties.[13] Among many heteroatoms, nitrogen, which has an atomic size comparable to that of neighboring carbon, has been the most widely employed heteroatom for the chemical doping of carbon nanomaterials leading to a modulated bandgap in graphene,[14] high electrochemical activity in carbon nanotubes,[15] tunable electron density, and enhanced photophysical properties in graphene quantum dots.[16] In addition, recent approaches have extended to the co-doping of heteroatoms to take advantage of the synergetic coupling effect between heteroatoms, which facilitates the modulation of doping efficiency, charge distribution, and enhanced optical properties.[17−19]

Judging by the current status of and potential for CDs, it is evident that the next step in the development of CDs will be tailoring the photophysical properties and elucidating the origin of PL in a controlled framework through a systematic study. To address these issues in the context of the synergetic inclusion of

Received: April 27, 2016
Revised: September 5, 2016
Published: September 6, 2016

ACS Publications © 2016 American Chemical Society

DOI: 10.1021/acs.chemmater.6b01710
Chem. Mater. 2016, 28, 6840−6847

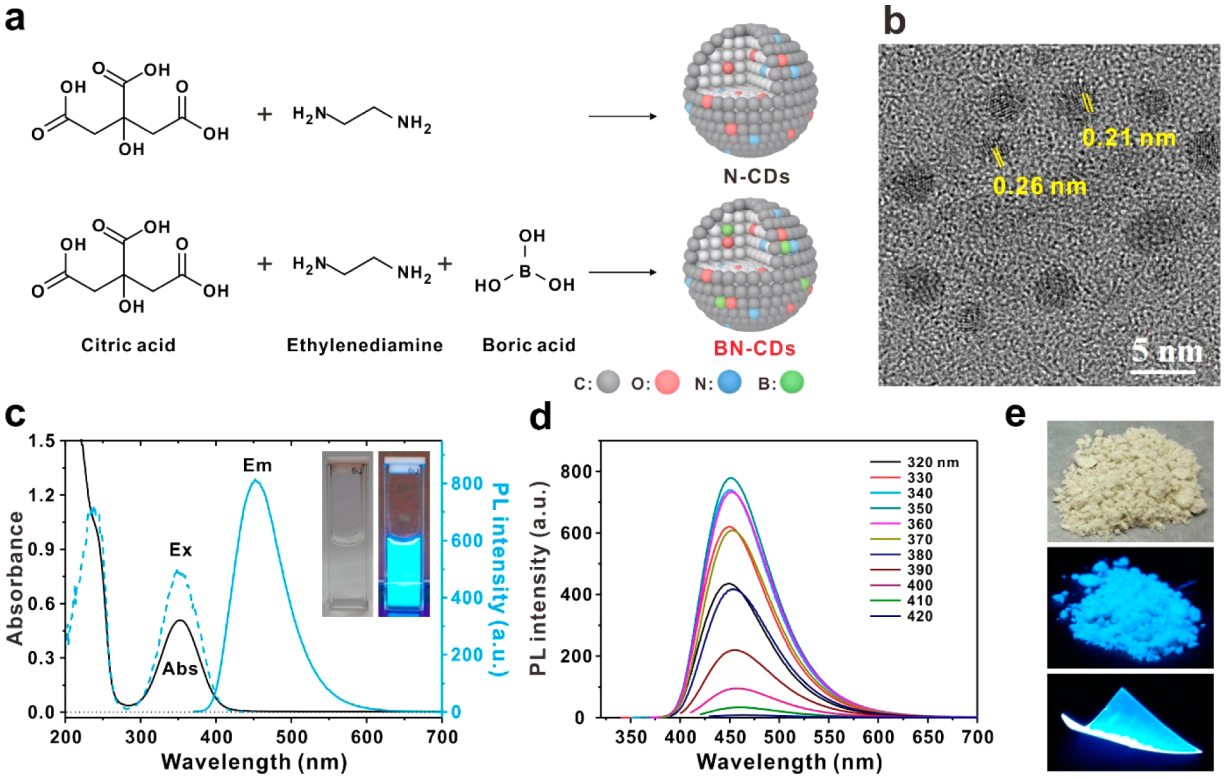

Figure 1. Synthesis and optical properties of BN-CD. (a) Synthetic scheme for N-CD and BN-CD. (b) High-resolution TEM image of BN-CD with the interlayer spacing measured. (c) UV−vis absorbance and photoluminescence spectra of BN-CD. Inset shows a BN-CD suspension (conc. 0.01 mg/mL) (left) under room light and (right) UV illumination at 365 nm. (d) Photoluminescence spectra of BN-CD under varying excitation wavelengths from 320 to 420 nm with 10 nm increments. (e) The bulk production of BN-CD powder and PVA film under daylight and UV illumination at 365 nm.

heteroatoms within the carbon frameworks, herein, we developed the boron-and-nitrogen co-doped CD (BN-CD) through a single-step microwave synthesis from small molecule precursors (Figure 1). For comparison, we prepared non-doped plain CD, N-doped CD (N-CD), and boron-doped CD (B-CD) as a control. Because of their graphitic structure, relatively uniform surface states, and less-abundant surface traps, the BN-CD displayed a significant quantum yield (QY), outperforming plain CD, N-CD, B-CD, and many other CDs reported to date (Tables S1 and S2). It is true that there are many precedents on the incorporation of heteroatoms in the CDs.

However, a detailed mechanistic framework was carefully developed in this study by using a series of spectroscopic analyses, including X-ray photoelectron spectroscopy and ultrafast spectroscopy, coupled with theoretical calculations based on density functional theory (DFT), revealing that the origin of the high photophysical property of the BN-CD is originated from its relatively abundant graphitic structures in the core and well-distributed surface states. Furthermore, single-molecule spectroscopy analysis confirmed the enhanced PL intensities and stabilities in a single BN-CD. We anticipate that this study will guide the future endeavor to uncover the full potential of CDs in various fields.

■ RESULTS AND DISCUSSION

As a main control set, N-CD was prepared through microwave pyrolysis using citric acid in the presence of ethylenediamine as a nitrogen source and a surface-passivating agent. In the case of BN-CD, boric acid was additionally introduced as a source of boron (Figure 1a). The high-resolution transmission electron microscopy (HR-TEM) image of the BN-CD revealed a quasi-spherical structure with an average diameter of 2.8 ± 0.5 nm and interlayer spacings of 0.21 and 0.26 nm, which matched the (100) and (020) facets of graphite (Figures 1b and S1). X-ray diffraction (XRD) patterns of BN-CD displayed a broad peak assigned to an interlayer spacing of 0.42 nm, which was greater than the value found between the planes of bulk graphite (0.344 nm), suggesting the presence of heteroatoms within the carbon framework (Figure S2).

N-CD showed two characteristic absorption peaks at 241 nm (sp^2-carbon network) and 351 nm ($n-\pi^*$ transition of carbonyl groups) (Figure S3). A shoulder peak at 420 nm was also observed, indicating the presence of lower energy states resulting from functional-surface states.[20] BN-CD showed similar absorption peaks, but uniquely without the long absorption tail above 420 nm (Figure 1c). The BN-CD solution exhibited bright blue emission under UV irradiation with a maximum emission centered at 450 nm upon excitation at 350 nm (Figure 1c). Interestingly, the emission spectrum of BN-CD showed excitation-independent behavior, whereas those of N-CD displayed excitation dependence (Figure 1d).

The excitation-wavelength dependent PL of CDs generally originates from a combination of quantum confinement effects and the distribution of different emissive states.[6] From the clear difference of excitation-wavelength dependent PL behaviors between BN-CD and N-CD at a similar narrow size distribution, it is plausible that the origin of the tunable PL of N-CD is not the quantum confinement effect but the intrinsic surface states. It also follows that the population of the surface states of BN-CD is significantly suppressed from the

DOI: 10.1021/acs.chemmater.6b01710
Chem. Mater. 2016, 28, 6840−6847

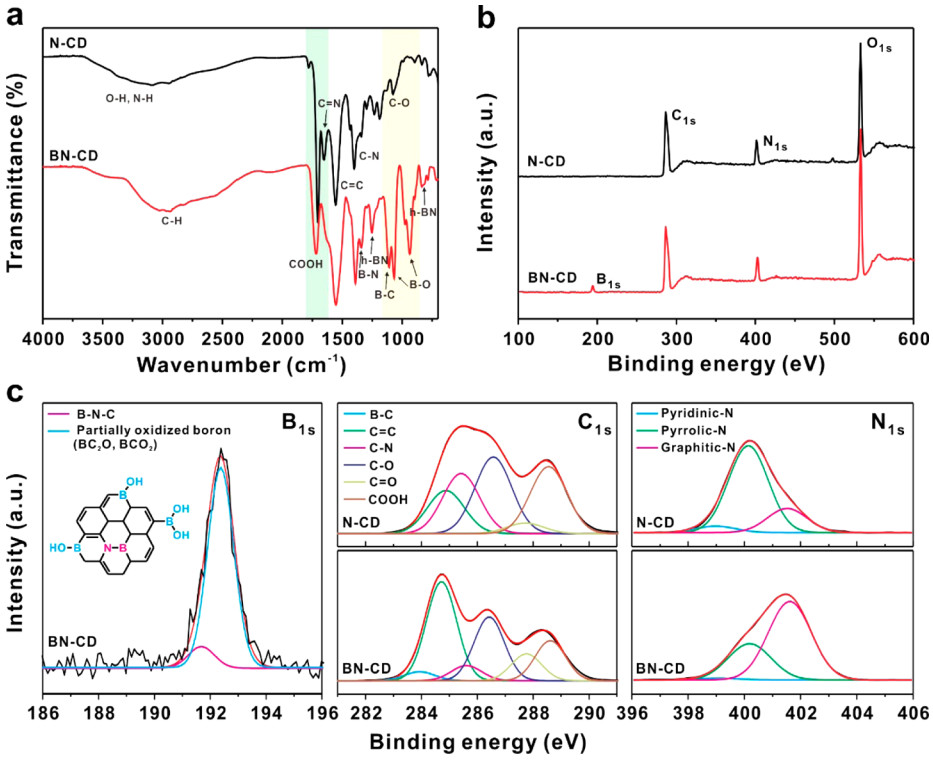

Figure 2. Chemical structures of N-CD and BN-CD. (a) FT-IR spectra and (b) XPS survey spectra of N-CD and BN-CD. (c) High-resolution XPS spectra of B 1s, C 1s, and N 1s of N-CD and BN-CD. The XPS survey spectrum indicates the presence of 3.51% B and 12.16% N in BN-CD.

absence of the absorption tail beyond 420 nm. The synthetic simplicity of the bulk production of desired CDs constitutes another advantage of CDs over other quantum dots, yielding multigram-scale powders in only 2 min (an average isolated yield exceeding 75%, Figure 1e). Unlike other CDs reported, the powder and the PVA film of BN-CD displayed intense blue PL under UV illumination, which can lead to potential application toward solid state devices (Figures 1e and S4). For example, QY of BN-CD powder exhibited 67.6%, whereas N-CD powder showed merely 1% (Table S3).

We further optimized the PL properties of BN-CD by controlling the molar ratio of boric acid to citric acid during the microwave pyrolysis (Figure S5). In general, the addition of boric acid during the synthesis improved the PL. The highest QY of BN-CD (80.8 ± 5.1%) was achieved with an equimolar concentration of each precursor and was almost twice as bright as that of N-CD (40.2 ± 1.8%), using an integrating-sphere method based on quinine sulfate as a reference. The optical properties of CDs were considerably changed after the incorporation of boron atoms within their network (Figure S6). Furthermore, non-doped plain CDs (CD) and boron-doped CD (B-CD) had only 2.1% and 1.2% of QY due to heterogeneous surface states from oxygen functional groups (Figure S7).

To investigate the chemical composition and structure of N-CD and BN-CD, FT-IR, elemental analysis (EA), and X-ray photoelectron spectroscopy (XPS) measurements were performed. Both CDs displayed characteristic IR peaks at 1086 cm^{-1} (C−O stretching), 1539 cm^{-1} (C═C stretching), and 2838 and 2929 cm^{-1} (C−H stretching) and a broad peak at approximately 3455 cm^{-1} (O−H and N−H stretching) (Figure 2a). In addition, the successful doping of boron in the carbon framework was confirmed by the appearance of new peaks corresponding to B−O, B−C, and B−N stretching in BN-CD.

According to EA and XPS, the major components of N-CD and BN-CD are C, N, and O. Interestingly, the ratios of C/N and C/O were decreased for BN-CD compared with those for N-CD because of an increased N doping ratio, which was aided by B doping in the carbon network (Figure 2b; Tables S4 and S5). Specifically, more nitrogen atoms, which are more-electronegative, were introduced to accommodate the charge density of the carbon matrix upon the introduction of less-electronegative boron atoms.[21]

In accord with the FT-IR result, the deconvoluted high-resolution XPS spectrum of B 1s in BN-CD also proved that B doping mostly occurs in the form of partially oxidized boron (BCO_2, BC_2O, 192.3 eV, 91.2%) with a minor contribution from B−N−C (191.5 eV, 9.8%) (Figure 2c).[22,23] In the high-resolution C 1s spectra, BN-CD and N-CD showed different fractions of carbon-related bonding with N and O species. For example, BN-CD contained increased fractions of C═C and C═O bonds (284.74 and 287.92 eV), whereas the fractions of C−N and COOH groups (285.77 and 288.79 eV) were reduced relative to sites resulting from the presence of fewer carboxylic acid groups and more carbonyl groups (Figure S8); this finding is in good agreement with the result of the theoretical study (see below).

Interestingly, the N 1s spectra also revealed different nitrogen configurations in BN-CD and N-CD (Figure 2c). Specifically, N-CD mainly consists of pyrrolic-N, whereas graphitic-N is the dominant nitrogen configuration in BN-CD (Figure S8). The different nitrogen constituents in N-CD and BN-CD indicate that graphitic-N plays an important role in enhancing the PL in CDs. On the basis of these results, we suggest that the graphitic structure and oxygen-related functional groups of CDs are closely connected to their PL properties. In particular, B-doping contributes to changing the configurations of the C and N bonding patterns, which in turn elevate the fraction of

DOI: 10.1021/acs.chemmater.6b01710
Chem. Mater. 2016, 28, 6840−6847

Table 1. Excited State Lifetime (τ) of N-CD and BN-CD in Aqueous Solution[a]

sample	λ_{em}[b] (nm)	time (ps)					τ_{avg}[d] (ps)
		τ_1[c] (A_1)	τ_2 (A_2)	τ_3 (A_3)	τ_4 (A_4)	τ_5 (A_5)	
N-CD	430	0.2 (80 ± 15%)	5.0 ± 0.7 (10 ± 1%)	330 (3%)	4990 (2%)	15 000 (5 ± 1%)	920 ± 100
	450		2.7 ± 0.3 (44 ± 3%)	330 (15 ± 1%)	4990 (8%)	15 000 (33 ± 1%)	5370 ± 180
	480		2.3 ± 0.7 (21 ± 4%)	330 (22 ± 2%)	4990 (10 ± 1%)	15 000 (47 ± 5%)	7580 ± 800
BN-CD	430	0.2 ± 0.1 (72 ± 30%)	2.5 ± 0.7 (10 ± 4%)	440 (3 ± 1%)		15 100 (15 ± 4%)	2230 ± 550
	450		1.5 ± 0.3 (25 ± 4%)	440 (10%)		15 100 (65 ± 3%)	9740 ± 410
	480		2.0 ± 2.1 (7 ± 4%)	440 (14 ± 1%)		15 100 (79 ± 4%)	11910 ± 660

[a]The fluorescence decay curves fitted to the multi-exponential function: $I(t)/I(0) = \Sigma_i^n A_i e^{-t/\tau_i}$. [b]Monitored emission wavelength. [c]Fractional amplitude. [d]The weight-averaged lifetime (τ_{avg}) obtained using the following equation: $\tau_{avg} = \Sigma_i^n A_i \tau_i$.

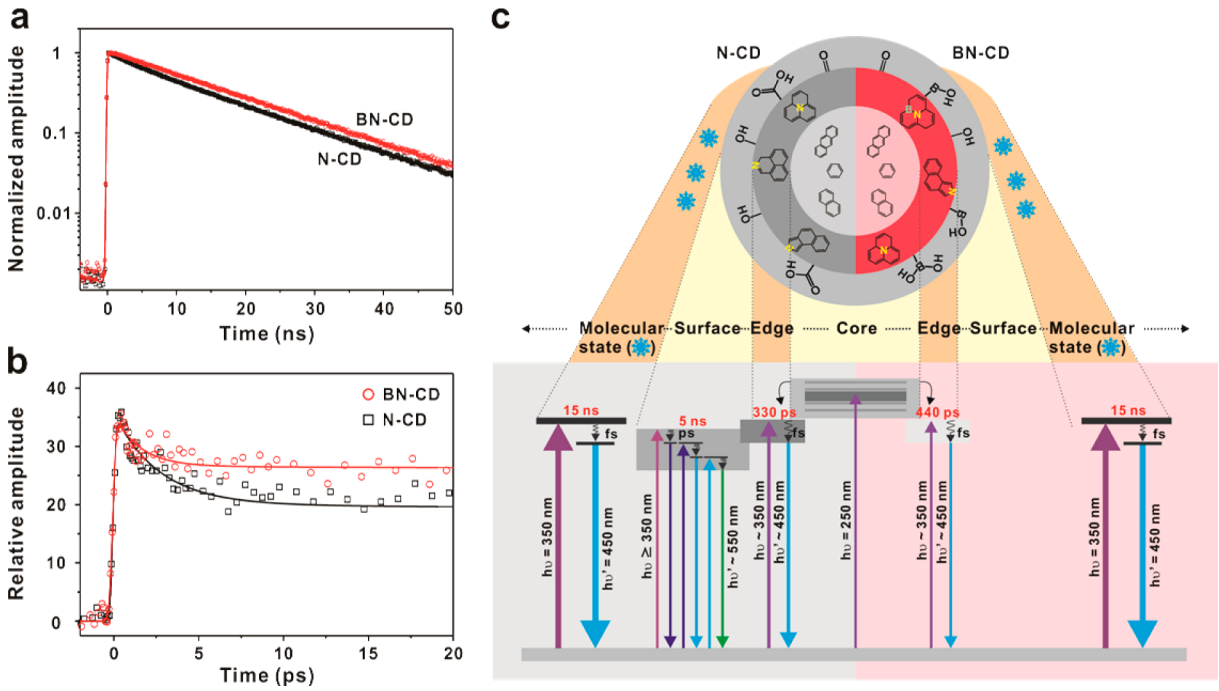

Figure 3. Photophysical properties of N-CD and BN-CD. (a) Normalized fluorescence decay profiles of CDs obtained by using TCSPC and monitored at 450 nm with excitation at 375 nm. The fits are also given in solid lines according to multi-exponential functions as $I(t) = A_3e^{-t/\tau_3} + A_4e^{-t/\tau_4} + A_5e^{-t/\tau_5}$ and $A_3e^{-t/\tau_3} + A_5e^{-t/\tau_5}$ for N-CD and BN-CD, respectively. (b) Femtosecond-resolved fluorescence decay kinetics of CDs measured using fluorescence upconversion and probed at 450 nm with excitation at 365 nm. From the fluorescence upconversion measurements, ultrafast decay components are screened corresponding to the time constants of τ_1 and τ_2 with the pre-exponential factors of A_1 and A_2, respectively. Note that the time scale is significantly different in (a) and (b). The designation of the pre-exponential factors (A_n) and time constants (τ_n) is given in Table 1. (c) The energy level diagram and schematic structures of the corresponding CDs with their relevant photophysical transitions.

graphitic-C and -N, generating well-distributed surface defect states and thus improving QY of BN-CD.

On the basis of the structural analysis, we propose that the high QY of BN-CD originates from its graphitic structure and less fraction of N-related defects. This assignment is independently supported by the fluorescence lifetime measurements of CDs. We investigated the ultrafast relaxation dynamics of CDs by measuring the emission lifetimes of BN-CD and N-CD. The representative results are listed in Table 1, obtained using both time-correlated single-photon counting (TCSPC) (Figures 3a and S9) and fluorescence upconversion spectroscopy to uncover the PL dynamics on different time scales (Figures 3b and S10). The overall results can be summarized as follows. First, a multitude of lifetime components were observed spanning a few hundred femtoseconds to a few tens of nanoseconds. Such components have several characteristic time scales: ~200 fs (τ_1), 2−5 ps (τ_2), 330−440 ps (τ_3), 5 ns (τ_4), and 15 ns (τ_5). This result suggests that either several competing deactivation pathways or a broad distribution of recombination rates exist in excited CDs.[24] Notably, the 5 ns lifetime component (τ_4) was unique to the N-CD sample. Second, the weight-averaged lifetime (τ_{avg}) was considerably shorter for N-CD than for BN-CD, which is in accordance with the lower QY of N-CD. For example, when compared at an emission wavelength of 450 nm, the ratio of the average lifetimes of N-CD and BN-CD was 0.55 ± 0.03, which is similar to the QY ratio of 0.67.

The temporal evolution of the PL of BN-CD was also investigated by time-resolved spectral measurements with picosecond accuracy (Table S6). Both N-CD and BN-CD have the common, longest lifetime component of ~15 ns, which could be attributed to the fluorescence lifetime of the molecule-like state of CDs. This assignment is based on the global-lifetime analysis to construct the deconvoluted spectra of this component, whose spectra and lifetime (15 ns) are very similar to those of imidazo[1,2*a*]pyridine-7-carboxylic acid,

DOI: 10.1021/acs.chemmater.6b01710
Chem. Mater. 2016, 28, 6840−6847

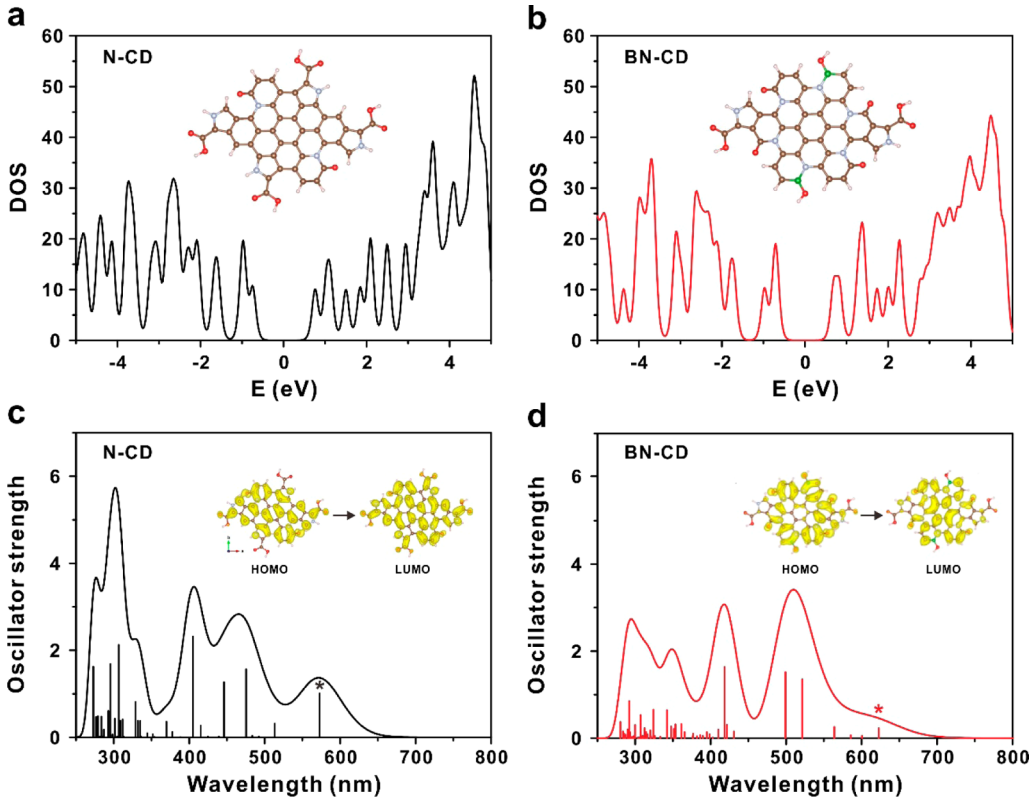

Figure 4. DFT calculations of N-CD and BN-CD. (a, b) Electronic densities of states (DOSs) and modeled structures for (a) N-CD and (b) BN-CD (brown, C; white, H; red, O; silver, N; green, B atoms). (c, d) The oscillator strengths with the raw data broadened by Gaussian functions (FWHM = 0.46 eV) for (c) N-CD and (d) BN-CD. The HOMO−LUMO absorption transitions with their charge distributions in the inset are marked with asterisks in each panel.

1,2,3,5-tetrahydro-5-oxo (IPCA) as described in recent reports.[25,26] The reduction of τ_{avg} in N-CD relative to BN-CD originated from the unique 5 ns component in N-CD at the partial expense of the longer 15 ns component. The lifetime of 5 ns is attributed to originate from surface states in N-CD, as evidenced by the additional absorption band around 450 nm.

The excitation of the surface states in N-CD is suggested to involve n−π* transitions of surface functional groups (oxygen-related) having non-bonding electrons. However, in BN-CD, those transitions can be suppressed because of the electron deficient nature of boron. As observed in Figure 2c, boron is mainly oxidized with oxygen-related functional groups. This assignment was further supported by examining the change in the 5 ns component when the excitation wavelength was tuned away from 375 nm to the red, where the surface states can be more excited (Figure S11). The time-resolved spectrum of the 5 ns component shows the same PL maxima as those of the several-hundred ps component with an additional shoulder band around 570 nm independent of excitation wavelength. The fraction of the 5 ns component, for instance, increased from 0.22 to 0.31 as the excitation wavelength was shifted from 375 to 450 nm; it further rose to 0.55 when excited at 510 nm.

We propose the several-hundred ps component (τ_3) originates from edge states. The edge state is designated to be different from the sp^2-core state and the surface, functional-group states in that this state is related to the boundary between sp^2- and sp^3-hybridized carbon and also to the surface exposed nitrogen such as that of a pyridinic group, undergoing n−π* transition with a similar energy gap to that of the molecular state.[27] The edge state abundant N-CD also contains the unique surface state. This can be rationalized in that the pyridinic N with non-bonding electrons is found more in N-CD than in BN-CD, as shown in Figure 2c. On the basis of the femtosecond fluorescence upconversion spectroscopy, the origins of the ∼200 fs (τ_1) and the 2−5 ps (τ_2) components in Table 1 are assigned to the intraband transitions and/or ultrafast hydration related to the solvent-exposed edge/surface states from their time scales.[28,29]

Taking these results together with all of the spectroscopic data, we correlate the shorter average-lifetime of N-CD with the relatively larger population of the edge and surface states existing in the N-CD to the reduction of QY compared to BN-CD, in which the formation of such states is minimized so that the PL mainly originates from the highly emissive molecular state of long lifetime (Figure 3c). In addition to the experimental investigations that account for the mechanism of the observed PL associated with the CD structure, we applied theoretical approaches based on DFT, using the Vienna Ab initio simulation package (VASP) with the Perdew−Burke−Ernzerhof (PBE) exchange correlation functional.

The optical transition properties were calculated using the time-dependent DFT method for the oscillator strength with B3LYP/6-31G* basis set (Figure 4; see the Supporting Information for the molecular models and computational details). The calculation is desirable indeed to involve the 3D model of CDs rather than plain 2D models that were undertaken in this study; however, on the basis of the experimental analyses, the sp^2-carbon cluster with heteroatom doping in a different arrangement and configurations are considered more critical in this study to support the observed

DOI: 10.1021/acs.chemmater.6b01710
Chem. Mater. 2016, 28, 6840−6847

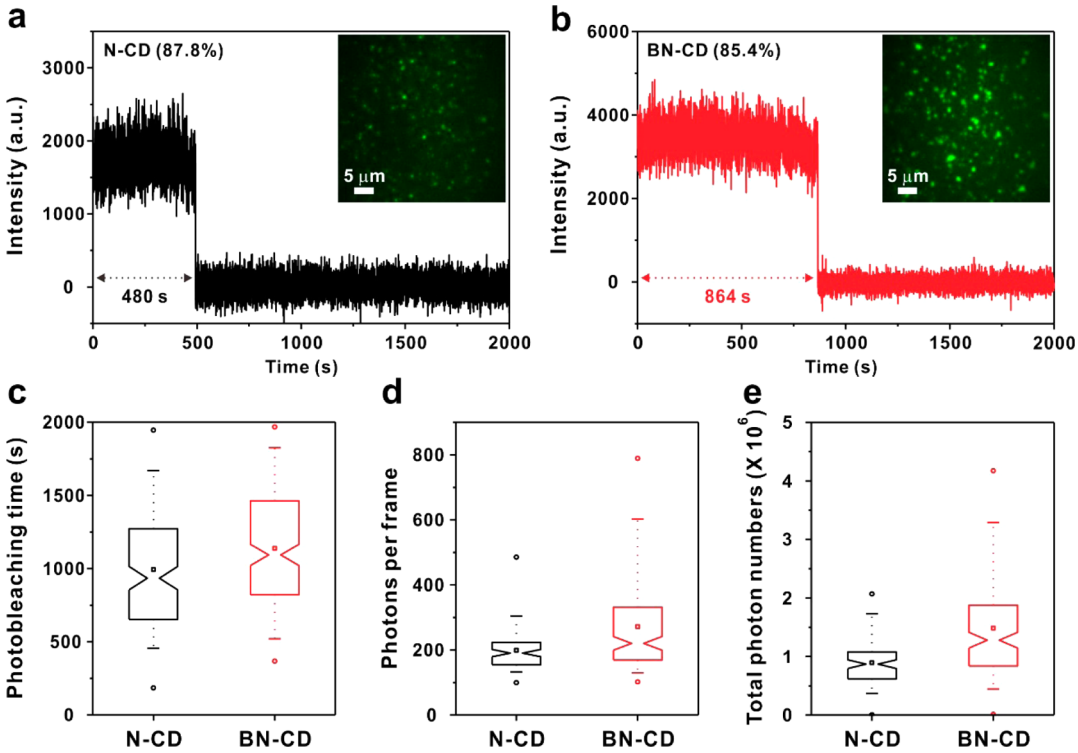

Figure 5. Single-molecule spectroscopy of N-CD and BN-CD. (a, b) Time-dependent photoluminescence traces of (a) single N-CD and (b) single BN-CD with a single-step photobleaching. The percentages were calculated from collection of N-CD (n = 311) and BN-CD (n = 225). Inset images are single N-CD and BN-CD under 375 nm illumination. (c−e) Box plot comparison of single N-CD and BN-CD bleached in one step: (c) single-step photobleaching time, (d) photons per frame, and (e) total photon numbers before photobleaching. The average single-step photobleaching times (τ_{avg}) were 993 ± 397 and 1138 ± 400 s for N-CD and BN-CD, respectively. The laser power was 50 W/cm^2, and the camera exposure time was 200 ms per frame. Spheres indicate minima and maxima. Squares indicate the average values, and notches represent the confidence interval at the confidence level of 95%.

enhancement in their photophysical differences between BN-CD and N-CD.

Our model structures, with various atomic configurations for N-CD and BN-CD, were constructed by combining the experimental results from FT-IR, EA, and XPS. The models involved a number of distinct functional groups and structures, such as carbonyl, carboxylic, B−OH, pyrrolic-N, and graphitic-N groups. As shown in Figure 4a, the most stable configuration of N-CD involved pyrrolic-N adjacent to a carboxylic acid group (COOH), with a minor contribution from graphitic-N located next to a carbonyl group (C═O) along the edge. This abundant pyrrolic-N configuration, however, did not influence the density of state (DOS) of N-CD, indicating that only graphitic-N is related to the optical properties of CDs. Conversely, in BN-CD, the most favorable atomic arrangement and configuration of boron occurred as B−OH with graphitic-N at edge sites, rather than within the carbon framework as B−N−C (Figure 4b). In addition, B−OH located next to graphitic-N serves similarly as the carbonyl group, affecting the PL properties of BN-CD (Figure S12). Moreover, the relative connectivity of the B−OH group with respect to C and N was important to the total energy; for example, when B−OH was near the edge site of N in the arrangement of C−N−B-OH, the total energy was lower than that of N−C−B-OH by 2.24 eV (Figure S13).

When the oscillator strengths of N-CD and BN-CD are correlated with the PL enhancement of BN-CD, our model depicted the lowest electronic transitions (HOMO to LUMO) at approximately 570 and 620 nm for N-CD and BN-CD, respectively (Figure 4c,d). The magnitude of the oscillator strength in BN-CD was approximately three times smaller than that of N-CD, as shown in the HOMO and LUMO models. These transitions (denoted with asterisks) involved the excitation of edge/surface states. It follows that the doping of B suppressed the excitation of the edge/surface states having relative short carrier recombination in BN-CD (Figure S14).

Ensemble spectroscopy studies often overlook single-particle behavior; therefore, we further characterized the photophysical properties of CDs at single-particle level using total internal reflection fluorescence microscopy (Figures 5 and S15). Individual particles of both N-CD and BN-CD demonstrated the stable PL intensity with a considerable fraction (more than 85%) of single-step photobleaching and a small fraction of multistep photobleaching behavior, when examining 311 particles of N-CD and 225 particles of BN-CD (Table 2). It is of note that both CDs exhibited no photoblinking phenomenon in which fluorescence intensities hop between

Table 2. Single-Particle Photoluminescence Behaviors of N-CD and BN-CD[a]

sample	bleaching (%)		
	one-step	two-step	three-step
N-CD	87.8[a]	11.6	0.6
BN-CD	85.4	13.3	10.3

[a]The percentages were calculated from 311 particles of N-CD and 225 particles of BN-CD measured individually.

DOI: 10.1021/acs.chemmater.6b01710
Chem. Mater. 2016, 28, 6840−6847

multiple levels. Stable PL of N-CD and BN-CD is in contrast with high PL fluctuations in previous studies of non-doped CDs,[20] but in accord with the reduced blinking by nitrogen doping.[30]

Moreover, time-dependent traces of single-step photobleaching in both CDs displayed significantly longer bleaching time (~1000 s) that is far beyond that of organic fluorophores and 1 or 2 orders of magnitude longer than those of non-doped CDs (Figure 5a,b).[20] Collectively, the average photobleaching times (τ_{avg}) including all single and multisteps were 818 ± 292 and 1053 ± 266 s for N-CD and BN-CD, respectively, under total internal reflection irradiation of 50 W/cm^2 laser beam (Table S7). In addition, the BN-CD showed an image of higher contrast compared to N-CD due to the increased lifetime and quantum yield under identical laser illumination (inset images in Figure 5a,b). To further confirm the origin of a higher PL in single BN-CD, we analyzed the total number of photons emitted before photobleaching for single-step bleaching traces, which constitutes the majority of single-particle traces over 85% (Figure 5c).

Individual characteristics of BN-CD showed modest improvement compared to those of N-CD. Especially, the average photon flux per camera frame (200 ms) was also increased from 200 ± 13 for N-CD to 275 ± 24 for BN-CD (Figure 5d). Collectively, BN-CD emitted more than a million photons, which is 60% larger than that of N-CD, resulting in the synergistic contribution to the higher PL observed (Figure 5e).

■ CONCLUSION

In summary, we developed a one-step synthesis of BN-CD with superior optical properties via the microwave pyrolysis of simple molecular precursors. BN-CD was characterized by various characterization techniques, including UV/vis, PL, HR-TEM, FT-IR, EA, and XPS. All methods conclusively supported the model of a graphitic core structure with more uniform surface states and fewer surface states in BN-CD, accounting for the observed PL enhancement of BN-CD over that of N-CD. Time-resolved ultrafast spectroscopy and DFT calculations further supported the CD structure involving heteroatom-tailored carbon networks. Furthermore, the single-molecule spectroscopy analysis indicated that high PL of BN-CD originates from the increased number of emitted photons per particle, compared to N-CD. We anticipate that this study will aid in uncovering the full potential of CDs as novel fluorophores for challenging bioimaging applications and optoelectronic devices in the future.

■ ASSOCIATED CONTENT

Supporting Information

The Supporting Information is available free of charge on the ACS Publications website at DOI: 10.1021/acs.chemmater.6b01710.

Experimental details and additional characterization data with figures and tables (PDF)

■ AUTHOR INFORMATION

Corresponding Author

*E-mail: bskim19@unist.ac.kr.

Notes

The authors declare no competing financial interest.

■ ACKNOWLEDGMENTS

This work was supported by the National Research Foundation of Korea (NRF) grants (NRF-2014R1A2A1A11052829, 2010-0028684, 2014R1A1A1003949, and 2011-0010186) and also by the Institute for Basic Science (IBS-R020-D1). B.R.L. acknowledges the support from the Engineering and Physical Sciences Research Council (UK).

■ REFERENCES

(1) Georgakilas, V.; Perman, J. A.; Tucek, J.; Zboril, R. Broad Family of Carbon Nanoallotropes: Classification, Chemistry, and Applications of Fullerenes, Carbon Dots, Nanotubes, Graphene, Nanodiamonds, and Combined Superstructures. *Chem. Rev.* **2015**, *115*, 4744−4822.

(2) Baker, S. N.; Baker, G. A. Luminescent Carbon Nanodots: Emergent Nanolights. *Angew. Chem., Int. Ed.* **2010**, *49*, 6726−6744.

(3) Li, X. M.; Rui, M. C.; Song, J. Z.; Shen, Z. H.; Zeng, H. B. Carbon and Graphene Quantum Dots for Optoelectronic and Energy Devices: A Review. *Adv. Funct. Mater.* **2015**, *25*, 4929−4947.

(4) Luo, P. J. G.; Yang, F.; Yang, S. T.; Sonkar, S. K.; Yang, L. J.; Broglie, J. J.; Liu, Y.; Sun, Y. P. Carbon-Based Quantum Dots for Fluorescence Imaging of Cells and Tissues. *RSC Adv.* **2014**, *4*, 10791−10807.

(5) Song, Y. B.; Zhu, S. J.; Yang, B. Bioimaging Based on Fluorescent Carbon Dots. *RSC Adv.* **2014**, *4*, 27184−27200.

(6) Zhu, S. J.; Meng, Q. N.; Wang, L.; Zhang, J. H.; Song, Y. B.; Jin, H.; Zhang, K.; Sun, H. C.; Wang, H. Y.; Yang, B. Highly Photoluminescent Carbon Dots for Multicolor Patterning, Sensors, and Bioimaging. *Angew. Chem., Int. Ed.* **2013**, *52*, 3953−3957.

(7) Choi, Y.; Kim, S.; Choi, M. H.; Ryoo, S. R.; Park, J.; Min, D. H.; Kim, B. S. Highly Biocompatible Carbon Nanodots for Simultaneous Bioimaging and Targeted Photodynamic Therapy In Vitro and In Vivo. *Adv. Funct. Mater.* **2014**, *24*, 5781−5789.

(8) Choi, Y.; Ryu, G. H.; Min, S. H.; Lee, B. R.; Song, M. H.; Lee, Z.; Kim, B. S. Interface-Controlled Synthesis of Heterodimeric Silver-Carbon Nanoparticles Derived from Polysaccharides. *ACS Nano* **2014**, *8*, 11377−11385.

(9) Li, H. T.; He, X. D.; Kang, Z. H.; Huang, H.; Liu, Y.; Liu, J. L.; Lian, S. Y.; Tsang, C. H. A.; Yang, X. B.; Lee, S. T. Water-Soluble Fluorescent Carbon Quantum Dots and Photocatalyst Design. *Angew. Chem., Int. Ed.* **2010**, *49*, 4430−4434.

(10) Wang, Y.; Kalytchuk, S.; Zhang, Y.; Shi, H. C.; Kershaw, S. V.; Rogach, A. L. Thickness-Dependent Full-Color Emission Tunability in a Flexible Carbon Dot Ionogel. *J. Phys. Chem. Lett.* **2014**, *5*, 1412−1420.

(11) Wang, L.; Zhu, S. J.; Wang, H. Y.; Qu, S. N.; Zhang, Y. L.; Zhang, J. H.; Chen, Q. D.; Xu, H. L.; Han, W.; Yang, B.; Sun, H. B. Common Origin of Green Luminescence in Carbon Nanodots and Graphene Quantum Dots. *ACS Nano* **2014**, *8*, 2541−2547.

(12) Sun, Y. P.; Zhou, B.; Lin, Y.; Wang, W.; Fernando, K. A. S.; Pathak, P.; Meziani, M. J.; Harruff, B. A.; Wang, X.; Wang, H. F.; Luo, P. J. G.; Yang, H.; Kose, M. E.; Chen, B. L.; Veca, L. M.; Xie, S. Y. Quantum-Sized Carbon Dots for Bright and Colorful Photoluminescence. *J. Am. Chem. Soc.* **2006**, *128*, 7756−7757.

(13) Paraknowitsch, J. P.; Thomas, A. Doping Carbons beyond Nitrogen: An Overview of Advanced Heteroatom doped Carbons with Boron, Sulphur and Phosphorus for Energy Applications. *Energy Environ. Sci.* **2013**, *6*, 2839−2855.

(14) Zhang, C. H.; Fu, L.; Liu, N.; Liu, M. H.; Wang, Y. Y.; Liu, Z. F. Synthesis of Nitrogen-Doped Graphene Using Embedded Carbon and Nitrogen Sources. *Adv. Mater.* **2011**, *23*, 1020−1024.

(15) Gong, K. P.; Du, F.; Xia, Z. H.; Durstock, M.; Dai, L. Nitrogen-Doped Carbon Nanotube Arrays with High Electrocatalytic Activity for Oxygen Reduction. *Science* **2009**, *323*, 760−764.

(16) Li, Y.; Zhao, Y.; Cheng, H. H.; Hu, Y.; Shi, G. Q.; Dai, L.; Qu, L. T. Nitrogen-Doped Graphene Quantum Dots with Oxygen-Rich Functional Groups. *J. Am. Chem. Soc.* **2012**, *134*, 15−18.

(17) Wang, S. Y.; Zhang, L. P.; Xia, Z. H.; Roy, A.; Chang, D. W.; Baek, J. B.; Dai, L. BCN Graphene as Efficient Metal-Free

DOI: 10.1021/acs.chemmater.6b01710
Chem. Mater. 2016, 28, 6840−6847

Electrocatalyst for the Oxygen Reduction Reaction. *Angew. Chem., Int. Ed.* **2012**, *51*, 4209−4212.
(18) Wang, X. W.; Sun, G. Z.; Routh, P.; Kim, D. H.; Huang, W.; Chen, P. Heteroatom-Doped Graphene Materials: Syntheses, Properties and Applications. *Chem. Soc. Rev.* **2014**, *43*, 7067−7098.
(19) Dong, Y. Q.; Pang, H. C.; Yang, H. B.; Guo, C. X.; Shao, J. W.; Chi, Y. W.; Li, C. M.; Yu, T. Carbon-Based Dots Co-doped with Nitrogen and Sulfur for High Quantum Yield and Excitation-Independent Emission. *Angew. Chem., Int. Ed.* **2013**, *52*, 7800−7804.
(20) Das, S. K.; Liu, Y. Y.; Yeom, S.; Kim, D. Y.; Richards, C. I. Single-Particle Fluorescence Intensity Fluctuations of Carbon Nanodots. *Nano Lett.* **2014**, *14*, 620−625.
(21) Choi, C. H.; Park, S. H.; Woo, S. I. Binary and Ternary Doping of Nitrogen, Boron, and Phosphorus into Carbon for Enhancing Electrochemical Oxygen Reduction Activity. *ACS Nano* **2012**, *6*, 7084−7091.
(22) Wu, Z. S.; Winter, A.; Chen, L.; Sun, Y.; Turchanin, A.; Feng, X. L.; Mullen, K. Three-Dimensional Nitrogen and Boron Co-doped Graphene for High-Performance All-Solid-State Supercapacitors. *Adv. Mater.* **2012**, *24*, 5130−5135.
(23) Iyyamperumal, E.; Wang, S. Y.; Dai, L. Vertically Aligned BCN Nanotubes with High Capacitance. *ACS Nano* **2012**, *6*, 5259−5265.
(24) Wen, X. M.; Yu, P.; Toh, Y. R.; Hao, X. T.; Tang, J. Intrinsic and Extrinsic Fluorescence in Carbon Nanodots: Ultrafast Time-Resolved Fluorescence and Carrier Dynamics. *Adv. Opt. Mater.* **2013**, *1*, 173−178.
(25) Song, Y. B.; Zhu, S. J.; Zhang, S. T.; Fu, Y.; Wang, L.; Zhao, X. H.; Yang, B. Investigation from Chemical Structure to Photoluminescent Mechanism: A Type of Carbon Dots from the Pyrolysis of Citric Acid and an Amine. *J. Mater. Chem. C* **2015**, *3*, 5976−5984.
(26) Zhu, S. J.; Zhao, X. H.; Song, Y. B.; Lu, S. Y.; Yang, B. Beyond Bottom-Up Carbon Nanodots: Citric-Acid Derived Organic Molecules. *Nano Today* **2016**, *11*, 128−132.
(27) Reckmeier, C. J.; Wang, Y.; Zboril, R.; Rogach, A. L. Influence of Doping and Temperature on Solvatochromic Shifts in Optical Spectra of Carbon Dots. *J. Phys. Chem. C* **2016**, *120*, 10591−10604.
(28) Kaniyankandy, S.; Achary, S. N.; Rawalekar, S.; Ghosh, H. N. Ultrafast Relaxation Dynamics in Graphene Oxide: Evidence of Electron Trapping. *J. Phys. Chem. C* **2011**, *115*, 19110−19116.
(29) Dhenadhayalan, N.; Lin, K. C.; Suresh, R.; Ramamurthy, P. Unravelling the Multiple Emissive States in Citric-Acid-Derived Carbon Dots. *J. Phys. Chem. C* **2016**, *120*, 1252−1261.
(30) Das, S. K.; Luk, C. M.; Martin, W. E.; Tang, L. B.; Kim, D. Y.; Lau, S. P.; Richards, C. I. Size and Dopant Dependent Single Particle Fluorescence Properties of Graphene Quantum Dots. *J. Phys. Chem. C* **2015**, *119*, 17988−17994.

DOI: 10.1021/acs.chemmater.6b01710
Chem. Mater. 2016, 28, 6840−6847